Desalination and Water Treatment
www.deswater.com

doi:10.5004/dwt.2018.23026

131 (2018) 252–260
November

Adsorption of Ag(I) in aqueous solution by polyamidoamine dendrimers functionalized magnetic graphene oxide

Ying-Xia Ma*, Ya-Lan Kou, Dan Xing, Peng-Sheng Jin, Wen-Jie Shao

State Key Laboratory of Advanced Processing and Recycling of Nonferrous Metals, School of Materials Science & Engineering, Lanzhou University of Technology, Lanzhou 730050, P.R. China, email: mayx2011818@163.com (Y.-X. Ma), kouyl930508@163.com (Y.-L. Kou), xingdanxdxd@163.com (D. Xing), jps11080705@163.com (P.-S. Jing), shaowenjie0809@163.com (W.-J. Shao)

Received 24 January 2018; Accepted 18 August 2018

ABSTRACT

In this study, the adsorption property of 3.0 generations polyamidoamine dendrimer functionalized magnetic graphene oxide (MGO-PAMAM-G3.0) for Ag(I) in aqueous solution was investigated by batch experiments and magnetic separation technology. The adsorption mechanism was studied by X-ray photoelectron spectroscopy (XPS), Fourier transform infrared spectroscopy (FT-IR) and N_2 adsorption/desorption isotherm. The effect of the adsorption conditions, such as pH, initial Ag(I) concentration, contact time and temperature on the adsorption property of MGO-PAMAM-G3.0 for Ag(I) was explored. The equilibrium data were analyzed using the Henry, Langmuir, Freundlich and Temkin isotherm models. The pseudo-first-order and pseudo-second-order adsorption kinetic models were employed to fit kinetics experimental data. The results showed that the main adsorption mechanism of MGO-PAMAM-G3.0 for Ag(I) was the formation of N-metal ions chemical complex and Ag(I) was reduced to element Ag in the adsorption process. The solution pH value had a major impact on adsorption Ag(I) with optimal removal observed around pH = 4.0–6.0 and the MGO-PAMAM-G3.0 was suitable for the adsorption low concentration Ag(I) from aqueous solution. The experimental data were better fitting of the Langmuir isotherm model and the pseudo-second-order equation, respectively.

Keywords: Magnetic graphene oxide; Polyamidoamine; Adsorption; Ag(I); Mechanism

1. Introduction

Silver, as the most widely used noble metal, has been applied in many industry fields such as electroplating, photography, coinage, ink formulation, mirroring, porcelain and metal alloy industries due to their prominent thermal and electrical conductivity, anti-bacterial and ornament performance [1,2]. Silver ions (Ag(I)) are harmful pollutants usually distributed in the lithosphere by their uses in various several industrial products. However, these industrial applications have generated wastewater containing large amount of Ag(I). Ag(I) is usually accumulated in living organisms (especially aquatic organisms) and causes numerous diseases and disorders through food chain [3]. Depending on the above severe detriment, the Integrated Wastewater Discharge Standard of China classifies silver as a primary pollutant, and its maximum discharge concentration is 0.5 mg/L [4]. In order to achieve the wastewater containing silver discharge standard, various methods have been used for Ag(I) removal from wastewater such as membrane filtration, chemical precipitation, ion exchange, solvent extraction and adsorption [5,6]. Adsorption method is knew as a lower costs, higher separation efficiency and ecofriendly treatment technique for the removal of various toxic heavy metal ions even at low concentration. Many adsorbents, such as activated carbon, resin, silica and chitosan [7] have been developed for the removal of Ag(I) from wastewater.

Graphene oxide (GO) is a kind of graphene-based material which is an ideal adsorbent due to its large specific surface areas and abundant oxygen-containing functional groups including hydroxyl, carboxyl and epoxy groups

*Corresponding author.

[8,9]. However, it is difficult to separate GO from aqueous solution on account of the well dispersity in water. Since magnetic separation has been considered as an effective method for solid liquid phase separation, Fe_3O_4 nanoparticles have been widely applied as adsorbents for the removal of contaminants from wastewater because of the simple and facile preparation process, high specific surface areas, relatively low cost, high adsorption capacity and easy manipulation by external magnetic field [10]. On the other hand, dendrimers are a type of hyper-branched polymers which are monodisperse macromolecules. Dendrimers have unique structures, including large number of surface functional groups, enormous specific surface areas in relation to volume, the presence of internal cavities and high degree of geometrical symmetry. Amine-terminated PAMAM dendrimers exhibit a high binding affinity for metal ions due to the coordination effect between tertiary amine, secondary amine and outer amino terminal of PAMAM and metal ions [11]. The supported materials decorated dendrimers used as adsorbents have recently received great attention. For example, silica-gel supported PAMAM dendrimers had been developed as an adsorbent for the adsorption of heavy metals such as Hg(II) and Co(II) [12,13]. The mesoporous silica (SBA-3, MCM-41, SBA-15 and MCM-48) supported PAMAM dendrimers is a kind of promising adsorbent, because of high level and uniform pore structure, pore volume, thermal and mechanical stability and versatility [14]. The PAMAM dendrimers functionalized various CNTs nanocomposites were prepared and applied for heavy metal ions (nickel, zinc, arsenic, cobalt) adsorption from industrial wastewater [15].

Considering the unique properties of GO, Fe_3O_4 nanoparticles as well as dendrimers, in our previous work [16], different generations of polyamidoamine dendrimers functionalized magnetic graphene oxide (MGO-PAMAM) were synthesized via step by step growth chemical graft approach and magnetic separation technology. The adsorption properties of the synthesized samples for Hg(II) in aqueous solution were investigated by batch experiments. The results showed that the MGO-PAMAM with generation 3.0 of dendrimers (MGO-PAMAM-G3.0) had the maximum adsorption capacity of 113.71 $mg \cdot g^{-1}$.

In order to determine the adsorption behavior and evaluate the feasibility for Ag(I) removal from aqueous solution, the effects of solution pH, initial Ag(I) concentration, contact time and temperature on the adsorption capacity of MGO-PAMAM-G3.0 were studied by batch experiments and magnetic separation technology in this work. In comparison to other adsorbents, the MGO-PAMAM-G3.0 has better biocompatibility, more adsorption sites for contaminant and easier separation by external magnetic field. It is worth mentioned that Ag(I) was reduced to element Ag in the adsorption process.

2. Experimental

2.1. Materials

Natural flake graphite (NFG) 60 BS mesh, with the purity of 99 wt% was supplied by Shandong Qingdao Tianhe Graphite Company (China). GO was prepared from NFG by the modified Hummers method [17]. Ethylenediamine (EDA), methyl acrylate (MA) and ethanediol were purchased from Tianjin Fuyu Chemical Co., Ltd. (China). Iron chloride hexahydrate ($FeCl_3 \cdot 6H_2O$), anhydrous sodium acetate (CH_3COONa), silver nitrate ($AgNO_3$), potassium persulfate ($K_2S_2O_8$) and potassium periodate (KIO_4) were purchased from Sinopharm Chemical Reagent Co., Ltd. (China). Nitric acid and sodium hydroxide (NaOH) were purchased from Tianjin Damao Chemical Co., Ltd. (China). MA was vacuum distilled in the rotary evaporation apparatus just before use. All of the other reagents are analytical grade and used as received without further purification.

2.2. Adsorbents preparation

MGO-PAMAM-G3.0 adsorbents were synthesized via step by step growth chemical grafting approach and magnetic separation technology according to our previous report [16]. Firstly, amino functionalized magnetic graphene oxide (MGO-NH_2) were obtained by one-pot solvothermal method using GO as carrier, $FeCl_3 \cdot 6H_2O$ as precursor, ethanediol as surfactant and reductant, sodium acetate as stabilizer, EDA as modifier and reductant in Teflon-lined stainless steel autoclave at 200°C for 8 h. Then, using the dry MGO-NH_2 as carrier, MA and EDA as functional monomers, MGO-PAMAM samples were prepared by Michael addition reaction and amidation condensation reaction under mechanical stirring at room temperature and N_2 protection environment. With the increasing of generation number, the amount of MA, EDA and the reaction time need to be increased to make the reaction process completely.

2.3. Characterization

Fourier transform infrared spectroscopy (FT-IR) of the samples recorded with a Nexus 670 (Thermo Electron Corporation, United States). The N_2 adsorption/desorption isotherm was performed by the Micromeritics ASAP 2020 (United States), and the specific surface area of sample was calculated by the Brunauer-Emmett-Teller (BET) method and the pore size distribution obtained from the Barret-Joner-Halenda (BJH) method. The X-ray photoelectron spectroscopy (XPS, Thermo Electron Corporation, United States) analysis carried out to detect the constituent elements of adsorbents before and after adsorption. Zeta potential was measured in a Malvern Zetasizer by dispersing the sorbent in distilled water with different pH values. The concentrations of Ag(I) in aqueous solution were determined using a UV-752N UV-vis spectrophotometer (Shanghai Precision Scientific Instrument Co., Ltd, China) by monitoring the absorbance at 365 nm at the presence of potassium periodate and potassium persulfate. The pH of solution was determined using a PHS-3C pH meter (Shanghai Leici Instrument Factory, China). The adsorption environment needed for the samples was provided by constant temperature oscillator of HZQ-211C (Shanghai Yiheng Technical Co., Ltd, China).

2.4. Adsorption experiments

Adsorption Ag(I) on MGO-PAMAM-G3.0 were carried out with typical batch experiments. All experiments were

performed in 250 mL conical flask containing 50 mL Ag(I) solution at 120 rpm and 298 K in a thermostat oscillator, after a desired period of adsorption, the adsorbent was removed out by a magnetic field and the Ag(I) content in the residual solution was measured by UV-vis spectrophotometer at 365 nm. The stock solution of Ag(I) (1,000 mg·L^{-1}) was prepared by dissolving a certain amount of $AgNO_3$ in distilled water. Working solutions were prepared by dilution of the stock solution to the desired concentration using distilled water. The adsorption parameters, including initial Ag(I) concentrations (10–80 mg·L^{-1}), initial pH (1.0–7.0), contact time (15–2880 min) and temperature (278–318 K) were investigated. The desired pH was obtained using HNO_3 and NaOH. Adsorption kinetic and isotherm experiments were conducted under the optimal adsorption conditions. The adsorption capacity and removal efficiency of Ag(I) onto the MGO-PAMAM-G3.0 were calculated using Eqs. (1) and (2), respectively [18]:

$$Q = \frac{(C_0 - C)\cdot V}{M} \quad (1)$$

$$R(\%) = \frac{(C_0 - C)\times 100}{C_0} \quad (2)$$

where Q (mg·g^{-1}) is the adsorption capacity of Ag(I), R(%) is the removal efficiency, C_0 and C (mg·L^{-1}) are the initial and residual concentration of Ag(I) in aqueous solution, respectively. V (L) is the volume of Ag(I) solution and M (g) is the mass of adsorbent used.

3. Results and discussion

3.1. Adsorption of Ag(I)

3.1.1. Effect of pH

The pH of the solution has been reported as a key condition that affects the adsorption property of adsorbent for heavy metal ions from aqueous solution [19]. The effect of solution pH on the adsorption of Ag(I) onto MGO-PAMAM-G3.0 was investigated in a wide range of 1.0–7.0 pH values and the results are presented in Fig. 1. It can be observed that the adsorption capacity of Ag(I) had little contribution in the pH range of 1.0–3.0. However, the adsorption capacity increased enormously with increasing in the pH range of 3.0–6.0, then reached a plateau value with pH range of 6.0–7.0. The above results could be explained by considering the H^+ competition for adsorption sites and the zero point of charge (pH_{zpc}) of the adsorbent. The pH_{zpc} was 6.2 for MGO-PAMAM-G3.0 presented in Fig. 1. We could see that the surface of MGO-PAMAM-G3.0 was positively charged when pH lower than 6.2. At lower pH values (1.0–3.0), most amine groups, which including tertiary amine, primary amine and –NH_2, were converted to protonated form lead to the number of negatively charged surface sites decreased and positively charged surface sites increased. The adsorption of MGO-PAMAM-G3.0 for Ag(I) was hampered by strong electrostatic repulsion, resulting to the lower adsorption capacity. Additionally, lower adsorption capacity of MGO-PAMAM-G3.0 for Ag(I) at acidic pH was due to the existence of a large number of H^+ competing with Ag(I) for the adsorption sites. With increasing of pH, the effect of H^+ on the adsorption could be ignored due to the concentration of H^+ decreased. Moreover, the electrostatic repulsion between Ag(I) and MGO-PAMAM-G3.0 reduced for deprotonation, making the adsorbents showed higher adsorption capacity for Ag(I). At the pH increased to 7.0 or higher, Ag(I) would combine with OH^- and form precipitation, which is not desirable to the following research of adsorption process.

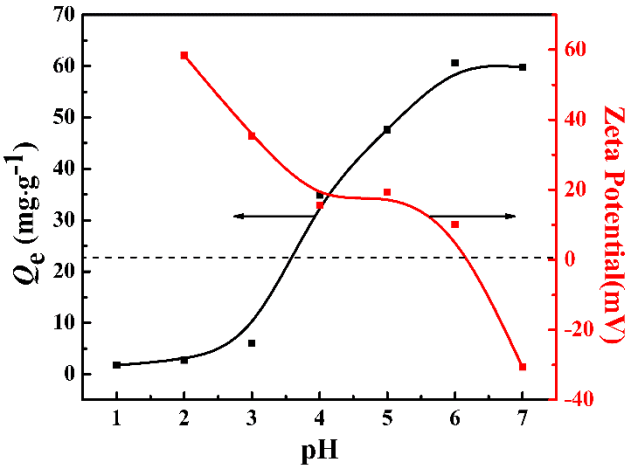

Fig. 1. Effect of solution pH on adsorption of MGO-PAMAM-G3.0 for Ag(I) (C_0 = 50 mg·L^{-1}, T = 298 K, t = 12 h, M = 25 mg) and Zeta potentials of MGO-PAMAM-G3.0.

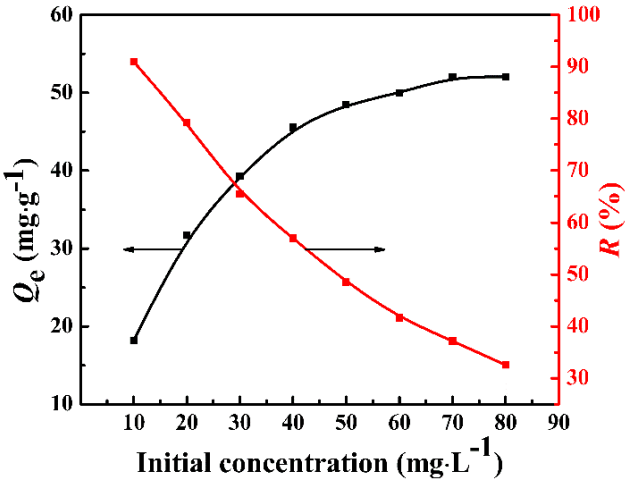

Fig. 2. Effect of initial concentration on adsorption of MGO-PAMAM-G3.0 for Ag(I) (T = 298 K, t = 12 h, pH = 6.0, M = 25 mg).

3.1.2. Effect of initial Ag(I) concentration

The effect of the initial Ag(I) concentration on the adsorption of MGO-PAMAM-G3.0 for Ag(I) was investigated. As shown in Fig. 2, the adsorption capacity increased obviously with increasing of initial concentration within 40 mg·L^{-1} and then tended to dynamic equilibrium. This was due to the increase of active sites on the adsorbent and the

greater driving force by a higher concentration gradient pressure. With the initial concentration continuing increase, the adsorption capacity did not significantly improve due to the saturation of the adsorbent surface with Ag(I). The maximum adsorption capacity of MGO-PAMAM-G3.0 for Ag(I) was 52.06 mg·g^{-1}. When the initial Ag(I) concentration was lower than 10 mg·L^{-1}, the removal efficiency could be higher than 90%, indicating that the low concentration of Ag(I) solution was beneficial to the adsorption of MGO-PAMAM-G3.0. Compared the maximum adsorption capacities of MGO-PAMAM-G3.0 with other GO-based adsorbents (Table 1), we can see that the adsorption capacity of MGO-PAMAM-G3.0 for heavy metal ions is higher than previous reported adsorbents [20–23].

Table 1
Adsorption capacities of GO-based adsorbents

Adsorbents	Adsorbed heavy metal ions	Q_{max} (mg·g^{-1})	References
GO-SS	Cu(II)	32.12	[20]
	Cd(II)	46.28	
	Nd(III)	38.17	
mGO/beads	Cr(VI)	1.90	[21]
GO-PER	Y(III)	32.38	[22]
	Nd(III)	49.88	
GO-G	Ni(II)	36.63	[23]
MGO-PAMAM-G3.0	Ag(I)	52.06	This work

3.1.3. Effect of contact time

Contact time is one of the important parameters for successful use of adsorbent in practical application. Fig. 3 shows the effect of contact time on the adsorption of Ag(I) onto MGO-PAMAM-G3.0. The result indicated that the adsorption capacity increased rapidly within the first 240 min and slowed down gradually with approaching equilibrium at 720 min.

3.1.4. Effect of temperature

Effect of the temperature on adsorption of MGO-PAMAM-G3.0 for Ag(I) is shown in Fig. 4. The adsorption capacity of MGO-PAMAM-G3.0 for Ag(I) increased significantly with an increase of temperature, then the adsorption capacity increased slowly from 298 K to 318 K, indicating that the higher temperature was beneficial to the adsorption of MGO-PAMAM-G3.0 for Ag(I) .

3.1.5. Adsorption kinetics

Kinetic models can be helpful to understand the mechanism of metal ions adsorption and evaluate property of the adsorbents. In order to further investigate the kinetic adsorption mechanism, the pseudo-first-order equation and pseudo-second-order equation, as shown in Eqs. (3) and (4), respectively, were employed to interpret the kinetic [24,25].

$$\ln\left(Q_e - Q_t\right) = \ln Q_e - k_1 t \tag{3}$$

$$\frac{t}{Q_t} = \frac{1}{k_2 Q_e^2} + \frac{t}{Q_e} \tag{4}$$

where Q_e (mg·g^{-1}) and Q_t (mg·g^{-1}) are the adsorption capacity of Ag(I) adsorbed at equilibrium and at time t (min), respectively, t is the contact time, k_1 (min^{-1}) and k_2 (g·min^{-1}·mg^{-1}) are the pseudo-first-order and pseudo-second-order rate constant, respectively.

The linear fitting results of the kinetic data shown in Fig. 5 and the corresponding adsorption kinetic model rate constants listed in Table 2. As shown in Fig. 5 and Table 2, the pseudo-second-order kinetic model (R^2 = 0.9996) gave a satisfactory fit to the experimental data compared to pseudo-first-order kinetic model (R^2 = 0.9705) for adsorp-

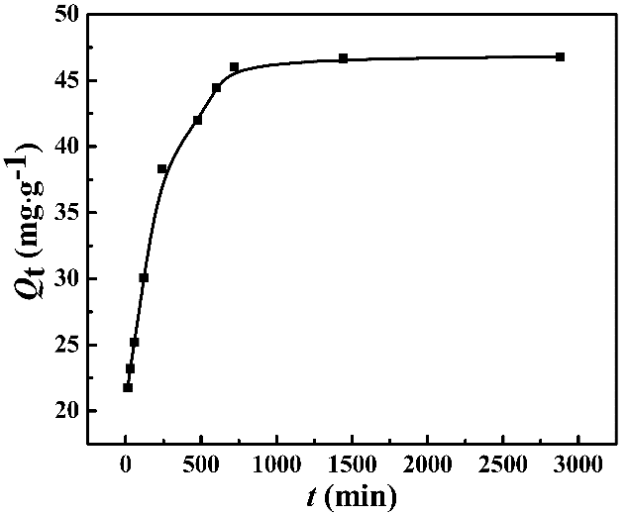

Fig. 3. Effect of contact time on adsorption of MGO-PAMAM-G3.0 for Ag(I) (C_0 = 40 mg·L^{-1}, T = 298 K, pH = 6.0, M = 25 mg).

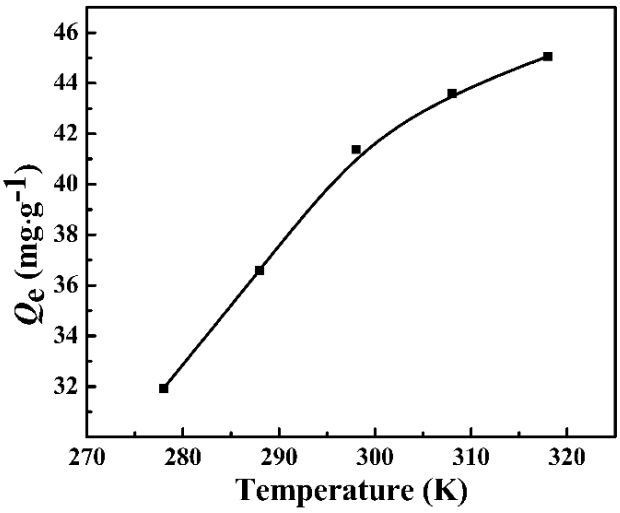

Fig. 4. Effect of temperature on adsorption of MGO-PAMAM-G3.0 for Ag(I) (C_0 = 40 mg·L^{-1}, t = 12 h, pH = 6.0, M = 25 mg).

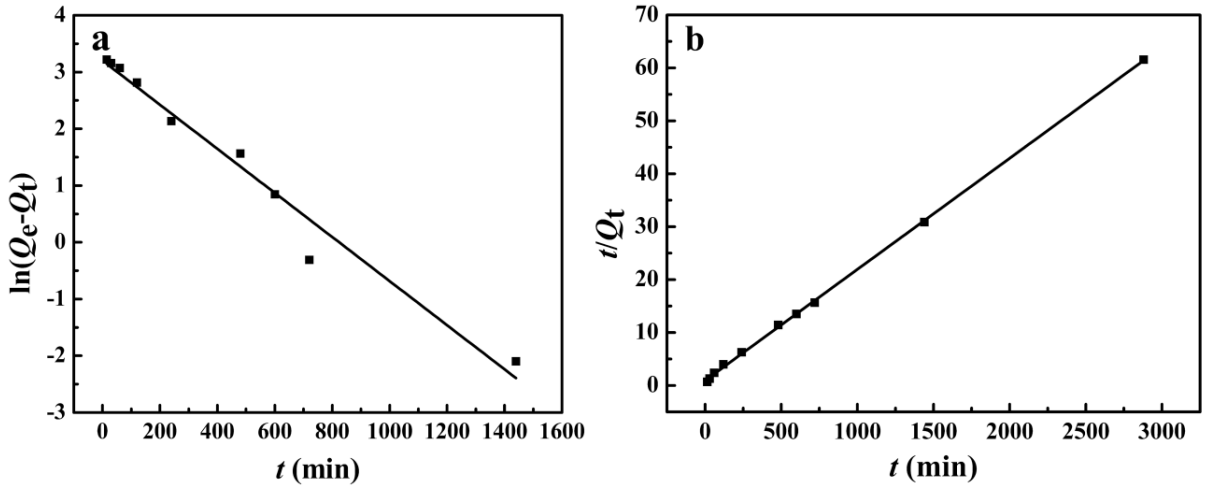

Fig. 5. Pseudo-first-order (a) and pseudo-second-order (b) kinetics of adsorption Ag(I) onto MGO-PAMAM-G3.0 (C_0 = 40 mg·L^{-1}, T = 298 K, pH = 6.0).

Table 2
Constants and correlation coefficients for the kinetic models of adsorption Ag(I) onto MGO-PAMAM-G3.0

Kinetic model	Parameter		R^2	Equation
Pseudo-first-order	k_1(min^{-1})	0.0039	0.9705	$\ln(Q_e-Q_t) = 3.2001 - 0.0039t$
	$Q_{e,cal}$ (mg·g^{-1})	24.54		
	$Q_{e,exp}$ (mg·g^{-1})	46.78		
Pseudo-second-order	k_2(g·min^{-1}·mg^{-1})	0.0005	0.9996	$t/Q_t = 0.0210t + 0.9321$
	$Q_{e,cal}$ (mg·g^{-1})	47.62		
	$Q_{e,exp}$ (mg·g^{-1})	46.78		

tion Ag(I) by MGO-PAMAM-G3.0, demonstrating that rate determining step of the adsorption process was mainly controlled by the chemical adsorption.

3.1.6. Adsorption isotherm

In order to well understand the adsorption behaviors, four isotherm equations were employed to analyze the adsorption isotherm data including the Henry, Langmuir, Freundlich and Temkin equations, which are expressed by Eqs. (5)–(8), respectively [26,27]:

$$Q_e = K_H C_e \tag{5}$$

$$\frac{C_e}{Q_e} = \frac{1}{K_L Q_{\max}} + \frac{C_e}{Q_{\max}} \tag{6}$$

$$\ln Q_e = \frac{1}{n}\ln C_e + \ln K_F \tag{7}$$

$$Q_e = \frac{RT}{b_T}\ln C_e + \frac{RT}{b_T}\ln A_T \tag{8}$$

where C_e (mg·L^{-1}) is the equilibrium concentration of Ag(I) in solution. Q_{max} (mg·g^{-1}) is the maximum adsorption capacity. K_H (L·g^{-1}), K_L (L·mg^{-1}) and K_F(mg·g^{-1}) are the Henry, Langmuir and Freundlich constants, respectively. n is the Freundlich exponent related to adsorption intensity, RT/b_T is related to the adsorption heat. A_T is the equilibrium constant corresponding to the maximum binding energy.

The fitting results obtained from these four adsorption models are shown in Fig. 6 and the calculated parameters are presented in Table 3. As can be seen in Fig. 6 and Table 3, the correlation coefficients (R^2) obtained from Langmuir model was higher than other three models, showing that the Langmuir model was more suitable to describe the adsorption isotherms. The maximum adsorption capacity (54.95 mg·g^{-1}) calculated from Langmuir model was closer to the experimental result (52.06 mg·g^{-1}). These results indicated that the adsorption of Ag(I) onto the surface of MGO-PAMAM-G3.0 took place by monolayer adsorption without any interaction between adsorbed ions, in other words, all the adsorption sites had equal adsorbate affinity and that the adsorption at one site did not affect the adsorption at an adjacent site [28].

3.2. Adsorption mechanism

The surface composition and the change of functional groups of the MGO-PAMAM-G3.0 before and after adsorption Ag(I) were analyzed by XPS. The XPS spectra of MGO-PAMAM-G3.0 before and after adsorption Ag(I) are presented in Fig. 7. The survey scan XPS spectra

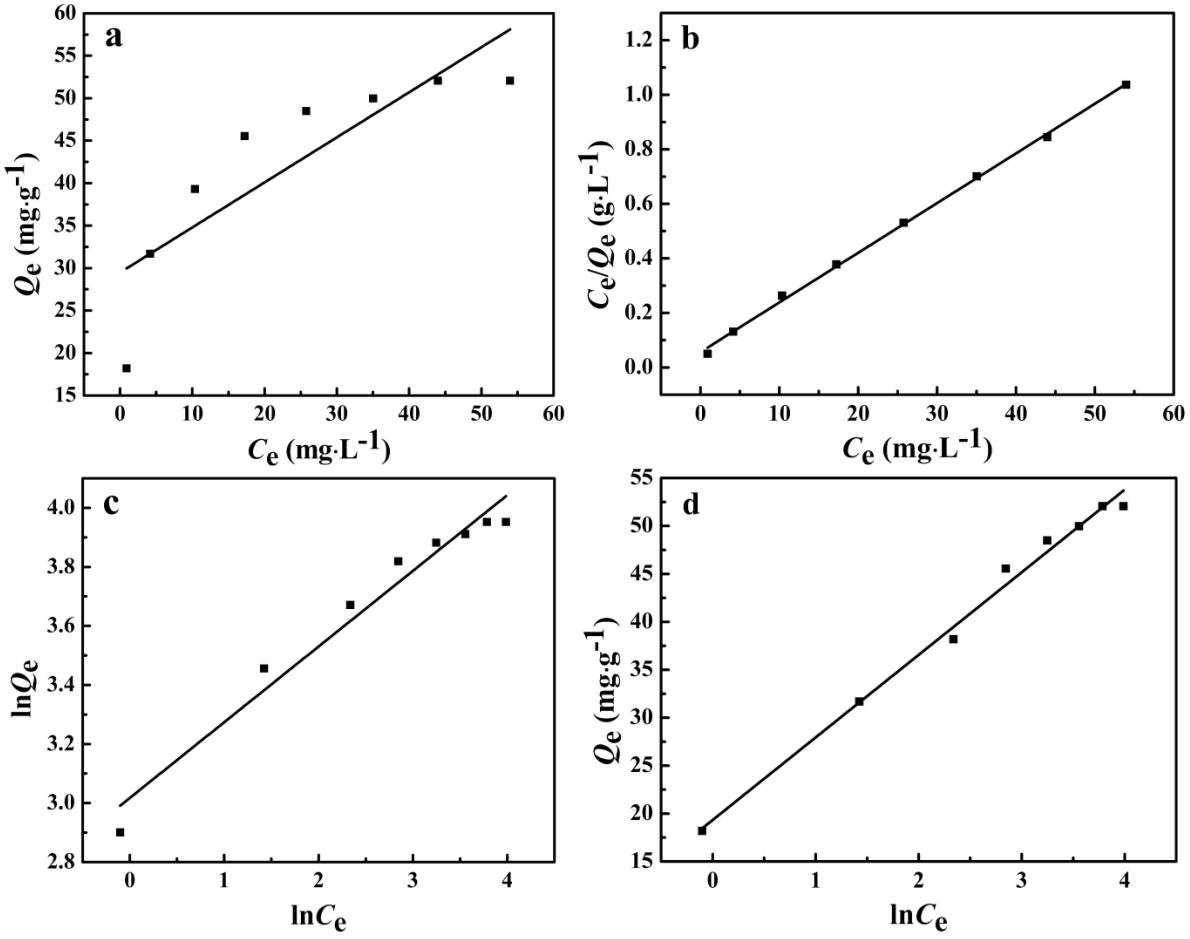

Fig. 6. Henry (a), Langmuir (b), Freundlich (c) and Temkin (d) adsorption isotherms of adsorption Ag(I) ontoMGO-PAMAM-G3.0 (T = 298 K, t = 12 h, pH = 6.0).

Table 3
Adsorption isotherm parameters of adsorption Ag(I) onto MGO-PAMAM-G3.0

Adsorption isotherm	Parameter		R^2	Equation
Henry	K_H (L·g^{-1})	0.5304	0.6796	$Q_e = 0.5304C_e$
Langmuir	K_L (L·mg^{-1})	0.3363	0.9984	$C_e/Q_e = 0.0189C_e + 0.0562$
	Q_{max} (mg·g^{-1})	52.91		
Freundlich	K_F (mg·g^{-1})	20.4381	0.9593	$\ln Q_e = 0.2564\ln C_e + 3.0174$
	n	3.9002		
Temkin	b_T	4.6711	0.9899	$Q_e = 0.5304\ln C_e + 29.4813$
	A_T	1.6996		

(Fig. 7a) of MGO-PAMAM-G3.0 before and after adsorption Ag(I) showed characteristic peaks of C 1s, O 1s, N 1s and Fe 2p. After adsorption Ag(I), a new peak for Ag 3d was observed at about 368 eV, suggesting the successful adsorption of Ag(I) on the surface of MGO-PAMAM-G3.0. Fig. 7b showed the high-resolution Ag 3d spectra, a pair of doublet-peaks assigned to Ag $3d_{3/2}$ and Ag $3d_{5/2}$ with binding energies at 374.2 eV and 368.2 eV, respectively, which was in accordance with silver in the Ag^0 oxidation state [3]. It suggested that Ag(I) adsorbed on the surface of MGO-PAMAM-G3.0 was reduced to elemental silver. The high-resolution C 1s spectra of MGO-PAMAM-G3.0 (Fig. 7c) could be divided into three peaks at 284.6 eV, 285.3 eV and 288.0 eV, belonging to the C-C, C-O/C-N and O=C-N species [29]. After adsorption Ag(I), the high-resolution C 1s spectra (Fig. 7d) didn't showany significant changes, indicating the existence form of C element remained the same for MGO-PAMAM-G3.0 before and after adsorption Ag(I). The characteristic peaks of the high-resolution O 1s spectra (Fig. 7e) appeared at 529.8 eV (O-Fe), 531.3

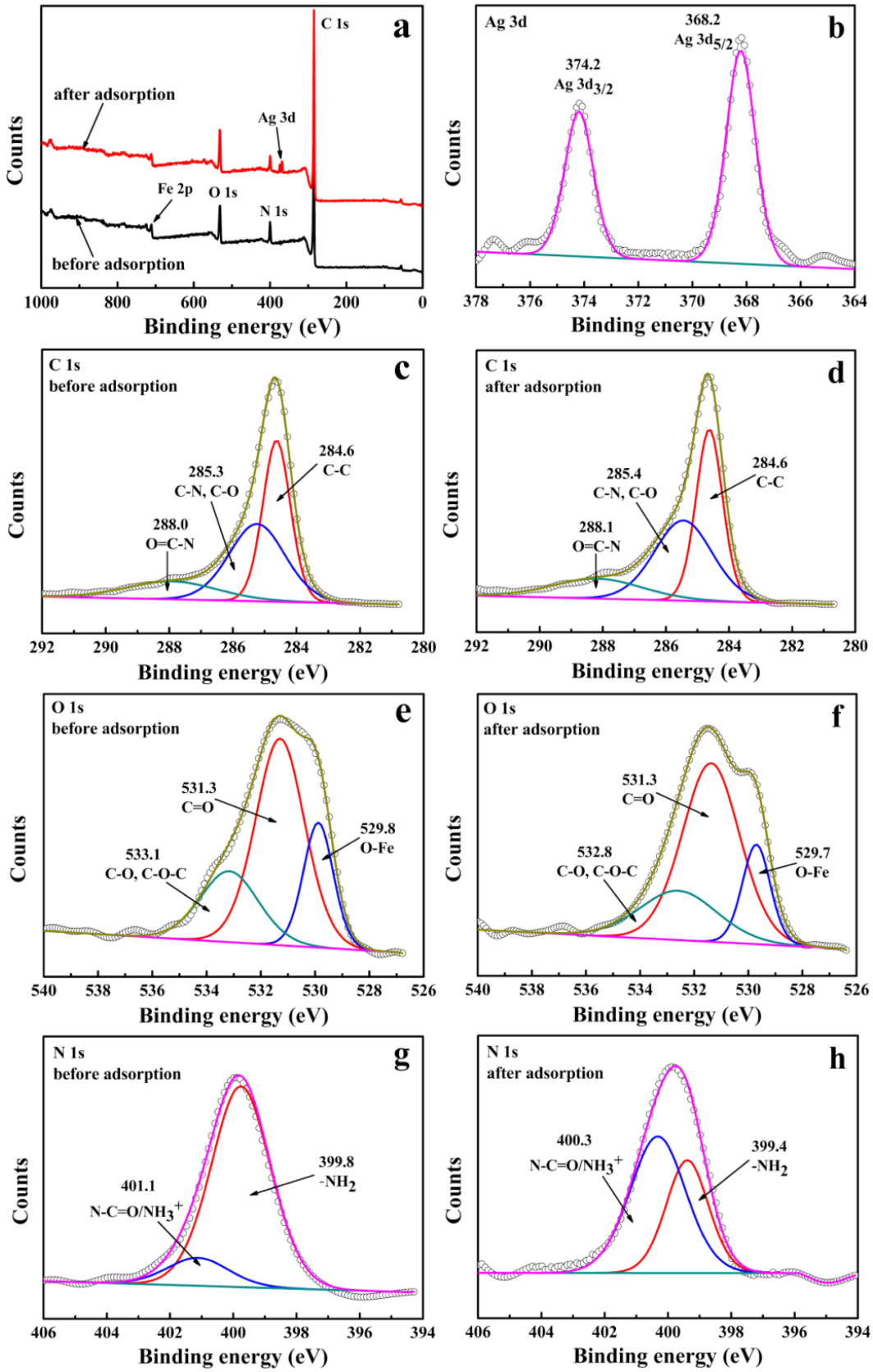

Fig. 7. The survey scan XPS spectra (a) and high-resolution scan XPS spectra of Ag 3d (b), C 1s (c, d), O 1s (e, f) and N 1s (g, h) of MGO-PAMAM-G3.0 before and after adsorption of Ag(I).

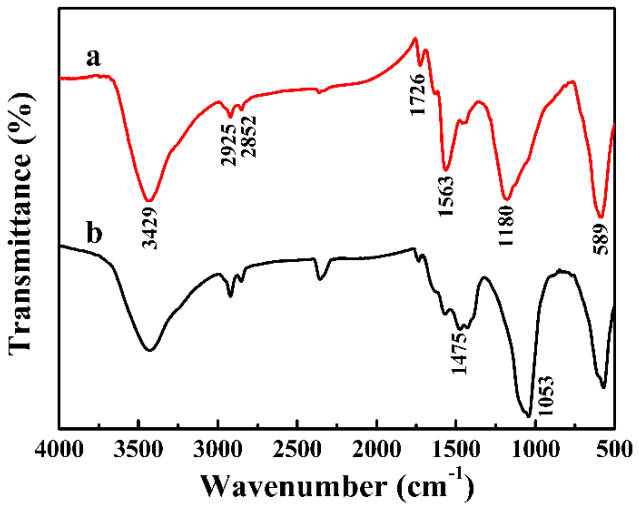

Fig. 8. FT-IR spectra of MGO-PAMAM-G3.0 before (a) and after (b) adsorption Ag(I).

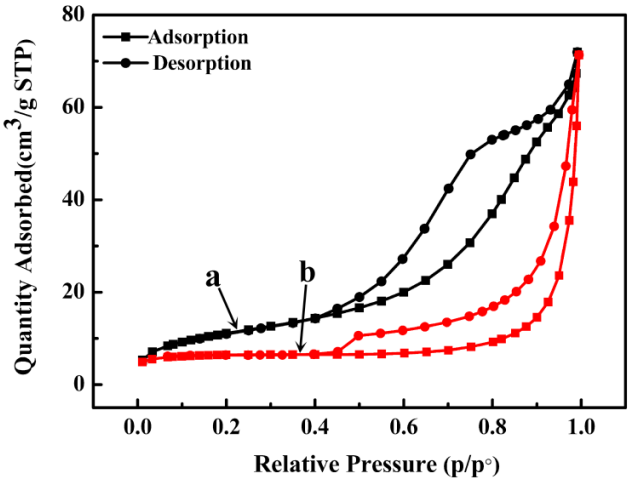

Fig. 9. N_2 adsorption/desorption isotherms of MGO-PAMAM-G3.0 before (a) and after (b) adsorption Ag(I).

eV (O=C) and 533.1 eV(O-C/C-O-C) [30]. After adsorption Ag(I), the peak position of O1s (Fig. 7f) almost did not change as well, indicating that the O element was not involved in the adsorption process. The high-resolution N 1s spectra of MGO-PAMAM-G3.0 before adsorption Ag(I) (Fig. 7g) shows two peaks appeared at binding energies of 399.8 eV and 401.1 eV were attributed to amines $–NH_2$ and amide bonds N-C=O/NH_3^+, respectively [31]. After adsorption Ag(I) (Fig. 7h), the two peaks were shifted to a lower binding energy due to the coordination interaction between amine groups and Ag(I). This phenomenon could be attributed to the formation of NH_2-Ag chemical complex, then nitrogen atom of NH_2-Ag chemical complex acquired electron via electron transport, resulting in increase in the density of its electron cloud. On the contrary, the Ag(I) became element silver as its lost electrons.

Fig. 8 shows the FT-IR spectra of MGO-PAMAM-G3.0 before (a) and after (b) adsorption Ag(I). The broad and strong band, ranging from 3200 cm^{-1} to 3600 cm^{-1}, was formed by the overlapping of the N-H bond of the amino groups and the O-H bond of the hydroxyl groups. The peaks at 2925 cm^{-1} and 2852 cm^{-1} could be ascribed to the C-H asymmetric and symmetric vibration of the $–CH_2$ groups. The peaks at 1563 cm^{-1} and 1180 cm^{-1} attributed to amide II (a combination peak of N-H bending and C-N stretching vibration) and C-N stretching vibration of tertiary amine, respectively [32]. The appearance of the peak around 1726 cm^{-1} was ascribed to the C=O stretching vibration of the amide in the MGO-PAMAM-G3.0. The peak at 582 cm^{-1} could be assigned to Fe-O stretching vibration of Fe_3O_4. Compared to Fig. 8a, in Fig. 8b the sharp and strong peak at 1563 cm^{-1} shifted to 1475 cm^{-1} and the peak intensity became weak. This phenomenon could be attributed to convert primary amine into secondary amine or tertiary amine due to interacting with $–NH_2$ and Ag(I).

The N_2 adsorption/desorption isotherms of MGO-PAMAM-G3.0 before (a) and after (b) adsorption Ag(I) are shown in Fig. 9. From Fig. 9 we can see that the isotherm curves of MGO-PAMAM-G3.0 show type-IV isotherm according to IUPAC classification, indicating the existence of mesoporous structures of samples. Calculating from the desorption branch of the nitrogen isotherm with BJH model, the specific surface area and the pore volume of MGO-PAMAM-G3.0 were 40.93 $m^2 \cdot g^{-1}$ and 0.110 $cm^3 \cdot g^{-1}$, respectively. This might be the gaps caused by Fe_3O_4 nanoparticles, PAMAM and GO sheets. After adsorption Ag(I), the specific surface area and the pore volume of sample decreased to 35.43 $m^2 \cdot g^{-1}$ and 0.108 $cm^3 \cdot g^{-1}$, respectively.

4. Conclusions

The MGO-PAMAM-G3.0 were successfully used as adsorbent for the removal low concentration of Ag(I) from aqueous solution by magnetic separation technology at pH in a range from 4.0 to 6.0, and higher temperature was beneficial to the adsorption of MGO-PAMAM-G3.0 for Ag(I) in aqueous solution.

Ag(I) was reduced to element Ag in the adsorption process of MGO-PAMAM-G3.0.

The adsorption process of MGO-PAMAM-G3.0 for Ag(I) was well described by the pseudo-second-order kinetics model and the Langmuir isotherm model, which revealed that the adsorption process was mainly considered as a monolayer chemical adsorption.

Acknowledgements

This work was supported by the National Natural Science Foundation of China (51403091) and the Postdoctoral Science Foundation of China (2015M572616).

References

[1] L.K. Fu, L.B. Zhang, S.X. Wang, Selective adsorption of Ag^+ by silica nanoparticles modified with 3-Amino-5-mercapto-1,2,4-triazole from aqueous solutions, J. Mol. Liq., 241 (2017) 292–300.

[2] L. Zhang, S.W. Yang, T. Han, Improvement of Ag(I) adsorption onto chitosan/triethanolamine composite sorbent by an ion-imprinted technology, Appl. Surf. Sci., 263 (2012) 696–703.
[3] Y.F. Zhao, D.F. Wang, H.Z. Xie, Adsorption of Ag(I) from aqueous solution by waste yeast: kinetic, equilibrium and mechanism studies, Bioproc. Biosyst. Eng., 38 (2015) 69–77.
[4] Y.L. Zhang, J. Yan, C.M. Dai, Sequestration of Ag(I) from aqueous solution as Ag(0) nanostructures by nanoscale zero valent iron (nZVI), J. Nanopart. Res., 17 (2015) 455–465.
[5] M. Firlak, M.V. Kahraman, E.K. Yetimoglu, Adsorption of Ag(I) ions from aqueous solutions using photocured thiol-Enehydrogel, Sep. Sci. Technol., 48 (2013) 2860–2870.
[6] B. Hayati, A. Maleki, F. Najafi, Super high removal capacities of heavy metals ($Pb^{2+}$and Cu^{2+}) using CNT dendrimer, J. Hazard. Mater., 336 (2017) 146–157.
[7] A. Maleki, B. Hayati, F. Najafi, Heavy metal adsorption from industrial wastewater by PAMAM/TiO_2 nanohybrid: preparation, characterization and adsorption studies, J. Mol. Liq., 224 (2016) 95–104.
[8] Z. Terzopoulou, G.Z. Kyzas, D.N. Bikiaris, Recent advances in nanocomposite materials of graphene derivatives with polysaccharides, Materials, 8 (2015) 652–683.
[9] G.Z. Kyzas, A. Koltsakidou, S.G. Nanaki, Removal of beta-blockers from aqueous media by adsorption onto graphene oxide, Sci. Total Environ., 537 (2015) 411–420.
[10] G.Z. Kyzas, N.A. Travlou, O. Kalogirou, Magnetic graphene oxide: effect of preparation route on reactive black 5 adsorption, Materials, 6 (2013) 1360–1376.
[11] C.H. Yen, H.L. Lien, J.S. Chung, Adsorption of precious metals in water by dendrimer modified magnetic nanoparticles, J. Hazard. Mater., 322 (2017) 215–222.
[12] X.T. Song, Y.Z. Niu, P.P. Zhang,Removal of Co(II) from fuel ethanol by silica-gel supported PAMAM dendrimers: combined experimental and theoretical study, Fuel, 199 (2017) 91–101.
[13] Y.Z. Niu, R.J. Qu, H. Chen, Synthesis of silica gel supported salicylaldehyde modified PAMAM dendrimers for the effective removal of Hg(II) from aqueous solution, J. Hazard. Mater., 278 (2014) 267–278.
[14] M. Mirzaie, A. Rashidi, H.A. Tayebi, Removal of anionic dye from aqueous media by adsorption ontoSBA-15/polyamidoamine dendrimer hybrid: adsorption equilibrium and kinetics, J. Chem. Eng. Data., 62 (2017) 1365–1376.
[15] B. Hayati, A. Maleki, F. Najafi, Synthesis and characterization of PAMAM/CNT nanocomposite as a supercapacity adsorbent for heavy metal (Ni^{2+}, Zn^{2+}, As^{3+}, Co^{2+}) removal from wastewater, J. Mol. Liq., 224 (2016) 1032–1040.
[16] Y.X. Ma, D. Xing, W.J. Shao, Preparation of polyamidoamine dendrimers functionalized magnetic graphene oxide for the adsorption of Hg(II) in aqueous solution, J. Colloid Interface Sci., 505 (2017) 352–363.
[17] L.Q. Guo, P.R. Ye, J. Wang, Three-dimensional Fe_3O_4-graphene macroscopic composites for arsenic and arsenate removal, J. Hazard. Mater., 298 (2015) 28–35.
[18] M. Ahmadi, H. Rahmani, B. Ramavandi, Removal of nitrate from aqueous solution using activated carbon modified with Fenton reagents, Desal. Water Treat., 76 (2017) 265–275.
[19] M. Tuzen, A. Sari, D. Mendil, Biosorptive removal of mercury(II) from aqueous solution using lichen (Xanthoparmeliaconspersa) biomass: kinetic and equilibrium studies, J. Hazard. Mater., 169 (2009) 263–270.
[20] J. Teng, X. Zeng, X. Xu, Assembly of a novel porous 3D graphene oxide-starch architecture by a facile hydrothermal method and its adsorption properties toward metal ions, Mater. Lett., 214 (2018) 31–33.
[21] H.C. Vu, A.D. Dwivedi, T.T. Le, Magnetite graphene oxide encapsulated in alginate beads for enhanced adsorption of Cr(VI) and As(V) from aqueous solutions: Role of crosslinking metal cations in pH control, Chem. Eng. J., 307 (2017) 220–229.
[22] B.Y. Yue, L.Y. Yu, F.P. Jiao, The fabrication of pentaerythritol pillared graphene oxide composite and its adsorption performance towards metal ions from aqueous solutions, Desal. Water Treat., 102 (2018) 124–133.
[23] F. Najafi, O. Moradi, M. Rajabi, Thermodynamics of the adsorption of nickel ions from aqueous phase using graphene oxide and glycine functionalized graphene oxide, J. Mol. Liq., 208 (2015) 106–113.
[24] X.T. Song, Y.Z. Niu, Z.M. Qiu, Adsorption of Hg(II) and Ag(I) from fuel ethanol by silica gel supported sulfur-containing PAMAM dendrimers: Kinetics, equilibrium and thermodynamics, Fuel, 206 (2017) 80–88.
[25] B. Song, P. Xu, G.M. Zeng, Modeling the transport of sodium dodecyl benzene sulfonate inriverine sediment in the presence of multi-walled carbon nanotubes, Water Res., 129 (2018) 20–28.
[26] B. Song, G.M. Zeng, J.L. Gong, Effect of multi-walled carbon nanotubes on phytotoxicity of sediments contaminated by phenanthrene and cadmium, Chemosphere, 172 (2017) 449–458.
[27] L.H. Hu, Z.P. Yang, L.M. Cui, Fabrication of hyperbranched polyamine functionalized graphene for high-efficiency removal of Pb(II) and methylene blue, Chem. Eng. J., 287 (2016) 545–556.
[28] Y.X. Ma, P.Q. La, W.J. Lei, Adsorption of Hg(II) from aqueous solution using amino-functionalized graphite nanosheets decorated with Fe_3O_4 nanoparticles, Desal. Water Treat., 57 (2016) 5004–5012.
[29] W.D. Xiao, B. Yan, H.B. Zeng, Dendrimer functionalized graphene oxide for selenium removal, Carbon, 105 (2016) 655–664.
[30] S.F. He, F. Zhang, S.Z. Cheng, Synthesis of sodium acrylate and acrylamide copolymer/GO hydrogels and their effective adsorption for Pb^{2+} and Cd^{2+}, ACS Sustain. Chem. Eng., 4 (2017) 3948–3959.
[31] S.Y. Zhou, A.L. Xue, Y. Zhang, Novel polyamidoamine dendrimer-functionalized palygorskite adsorbents with high adsorption capacity for Pb^{2+} and reactive dyes, Appl. Clay Sci., 107 (2015) 220–229.
[32] J. Ederer, P. Janos, P. Ecorchard, Determination of amino groups on functionalized graphene oxide for polyurethane nanomaterials: XPS quantitation vs. functional speciation, RSC Adv., 7 (2017) 12464–12473.